

---

Customized computer models of eyes  
with intraocular lenses. 8

---

---

## *8. Customized computer models of eyes with intraocular lenses*

---

This chapter is based on the article by Rosales. P et al., “*Customized computer models of eyes with intraocular lenses*” Optics Express, Vol. 15, pp.2204-2218. Coauthors of the study is S. Marcos. The contribution of Patricia Rosales to the study was to measure tilt and decentration and experimental aberrations (together with Lourdes Llorente) in patients with intraocular lenses, to measure simulated aberrations with customized computer model eyes and to analyze the results for the same patients.

## ***RESUMEN***

***Objetivos:*** Elaborar un modelo de ojo computacional individualizado con el fin de poder predecir las aberraciones oculares y evaluar la calidad óptica de ojos pseudofáquicos con lentes intraoculares implantadas.

***Métodos:*** A partir de datos individualizados de topografía corneal, el ángulo  $\lambda$ , biometría ocular, geometría de la lente intraocular implantada, inclinación y descentramiento de la lente intraocular medida para cada ojo, se elaboró un modelo de ojo en Zemax con el que se calcularon las aberraciones totales y corneales para cada ojo sin considerar el tilt y el descentramiento de la lente intraocular y teniéndolos en cuenta. Las aberraciones oculares obtenidas de la simulación se compararon con las obtenidas experimentalmente mediante trazado de rayos láser (LRT) en estos ojos de pacientes con lentes intraoculares implantadas.

***Resultados:*** Las aberraciones individuales más relevantes se predicen bien con el modelo de ojo completo. La aberración esférica corneal y el coma horizontal se compensan por efecto de la lente intraocular, y en un 58.3% de los casos, la inclinación y el descentramiento de la lente intraocular contribuyen a la compensación del coma horizontal.

***Conclusiones:*** Los modelos de ojo computacionales individualizados son una buena representación de ojos reales con lentes intraoculares implantadas y permiten comprender la contribución relativa de factores ópticos, geométricos y factores relacionados con la cirugía en la calidad de la imagen. Aunque la aberración esférica corneal se reduce con la lente intraocular esférica, otras aberraciones de alto orden todavía siguen afectando a las aberraciones totales en ojos pseudofáquicos. La inclinación y el descentramiento de las lentes intraoculares tienen poca influencia en la calidad óptica total del ojo.

## ***ABSTRACT***

***Purpose:*** To present a customized computational model eye to predict the ocular aberrations and to evaluate the optical quality of pseudophakic eyes with implanted intraocular lenses.

***Methods:*** A model eye was built in Zemax with customized data of each pseudophakic eye obtained from corneal topography,  $\lambda$  angle, ocular biometry, implanted intraocular lens geometry, tilt and decentration of the IOL measured for each eye, to calculate the simulated corneal and total aberrations for each eye without considering IOL's tilt and decentration and taking it into account. Simulated aberrations were compared with those obtained experimentally from laser ray tracing technique measured on the same eyes.

***Results:*** Relevant individual aberrations were well predicted by the complete eye model. Corneal spherical aberration and horizontal coma were compensated by the IOL, and in 58.3% of the cases, IOL tilt and decentration contributed to compensation of horizontal coma.

***Conclusions:*** We conclude that customized computer eye models are a good representation of real eyes with IOLs and allow understanding the relative contribution of optical, geometrical and surgically-related factors to image quality. Corneal spherical aberration is reduced by aspheric IOLs, although other corneal high order aberrations are still a major contributor to total aberrations in pseudophakic eyes. Tilt and decentration of the IOLs represent a relatively minor contribution of the overall optical quality of the eye.

## 1. INTRODUCTION

Schematic eye models have been used for decades to represent paraxial properties of the ocular optics and, in some cases, to describe general trends for symmetric aberrations. Those schematic eyes are based on average anatomic data of the eye and rely on several simplifications. For example, paraxial schematic eyes of Gullstrand, Le Grand, Emsley or Rabbetts (See Atchison and Smith for a review (Atchison & Smith, 2000)), with spherical surfaces, are unable to predict the amounts of spherical aberrations found in real eyes. More sophisticated eye models are improved by aspherizing one or more surfaces or by including a gradient index distribution in the crystalline lens, such as those of Lotmar, Kooijman, Liou and Brennan (See Atchison and Smith for a review (Atchison & Smith, 2000)). In general, modifications of schematic eye models are proposed for specific purposes. For example, the eye of Liou and Brennan was designed to give a realistic spherical aberration, and off-axis monochromatic aberrations were not considered. In some cases a geometrical property of the ocular components in the model is adjusted to reproduce observed optical performance under different conditions (i.e. change of spherical aberration with accommodation (Navarro, Santamaría & Bescós, 1985), or off-axis aberrations across the visual field (Escudero-Sanz & Navarro, 1999)).

Today, the aberrations of the eye can be reliably measured with ocular aberrometers, and there is a deeper understanding on their change with different conditions (i.e. aging (McLellan, Marcos & Burns, 2001), accommodation (He, Burns & Marcos, 2000) or surgical interventions (Barbero, Marcos & Jimenez-Alfaro, 2003)). The fact that the amount and spatial distribution of aberrations vary widely in the population (Castejon-Mochon, Lopez-Gil, Benito & Artal, 2002, Thibos, Hong, Bradley & Cheng, 2002) prevents one simple eye model from representing the actual optical performance of real eyes. In addition to the description and measurement of the ocular aberrations, there is an increasing interest in understanding the causes for the optical aberrations of the individual eyes (Marcos, Burns, Prieto, Navarro & Baraibar, 2001). This interest has been paralleled by the development of new instrumentation to measure the geometrical and structural properties of the ocular components (topography of the anterior and posterior corneal surfaces (Dubbelman, Sicam & van der Heijde, 2006) , optical biometry (Drexler, Baumgartner, Findl, Hitzenberger, Sattmann & Fercher,

1997), phakometry (Garner, 1997, Mutti, Zadnik & Adams, 1992), anterior and posterior lens geometry (Dubbelman & van der Heijde, 2001, Dubbelman, van der Heijde & Weeber, 2001, Koretz, Cook & Kaufman, 2001), or lens tilt and decentration (Barry, Dunne & Kirschkamp, 2001, Phillips, Perez-Emmanuelli, Rosskothén & Koester, 1988, Rosales & Marcos, 2006). The combinations of the above measurements allows understanding of phakic ocular development and changes to the ocular condition. Moreover, the new directions for improving the performance of corneal refractive surgery, and intraocular and contact lens design, and particularly the increase of individually customized approaches for correction require more sophisticated eye models, using real individual data of the eye under study.

To model individual eyes is a complex task because it requires accurate biometric eye data, such as the shape of the ocular surfaces, knowledge of the gradient index distribution of the crystalline lens, position of the lens and the position of the fovea. The study of optical performance of pseudophakic eyes, where the natural crystalline lens has been replaced with an intraocular lens (IOL), is particularly interesting. On one hand, the complexity of the eye models can be somewhat reduced, since the intraocular lens has constant index and the shape of the surfaces and optical design is accessible. Identifying the relative contribution of different factors to the optical quality in pseudophakic eyes is helpful to evaluate the real impact of new IOL designs and the potential need of improvement of surgical strategies in cataract surgery. Most studies to date are either based on simple eye models (Atchison, 1989, Atchison, 1990, Holladay, Piers, Koranyi, van der Mooren & Norrby, 2002) or are limited to a global description of optical performance through double-pass (Artal, Marcos, Navarro, Miranda & Ferro, 1995, Guirao, Redondo, Geraghty, Piers, Norrby & Artal, 2002) or aberration measurements (Barbero et al., 2003, Marcos, Barbero & Jiménez-Alfaro, 2005, Mester, Dillinger & Anterist, 2003, Rocha, Soriano, Chalita, Yamada, Bottós, Bottós, Morimoto & Nosé, 2006). Most of the theoretical studies have concentrated on the impact of lens geometry on spherical aberration. The effect of tilt and decentration of the intraocular lens has been discussed by Atchison (Atchison, 1990) and Holladay (Holladay et al., 2002) based on theoretical models. Barbero (Barbero et al., 2003) compared optical aberrations of spherical intraocular lenses measured in vivo with the measurements on same lenses in vitro using laser ray tracing, and estimations from virtual ray tracing using customized computer eye models (incorporating corneal topography, IOL geometry and anterior chamber depth). While the three techniques provided similar

estimates of spherical aberration, third and higher order aberrations were not correctly predicted, since, as shown both in vitro and numerically, they were affected by the actual amounts and combinations of IOL tilt and decentration. Finally, the relevant contribution of corneal optics to overall optical quality, and particularly the systematic induction of high order aberrations (trefoil and tetrafoil) in cataract surgery has also been emphasized as described in Chapter 7 (Guirao, Tejedor & Artal, 2004, Marcos, Rosales, Llorente & Jiménez-Alfaro, 2007, Pesudovs, Dietze, Stewart & Cox, 2005).

In this Chapter we present a customized model eye in patients with intraocular lenses of known geometry where tilt and decentration values have been measured in vivo. Experimental measurements of ocular aberrations in these eyes are compared with estimates of aberrations from numerical ray tracing using a customized model eye, where individual measurements of post-operative corneal topography, anterior chamber depth, IOL geometry, IOL tilt and decentration and the misalignment of the line of sight are used. This study will allow validation of the accuracy of customized eye models to predict measured aberrations, to investigate the contribution of the different components to overall image quality in eyes with IOLs and to assess the real benefits of new IOL designs.

## 2. METHODS

### 2.1 Subjects

The study was performed on 12 eyes of 7 subjects (average age  $71.23 \pm 3.52$  yrs, mean and standard deviation) implanted with aspheric IOLs (Acrysof IQ, Alcon) of known geometry in a standard phacoemulsification surgical procedure with a 3.2-mm superior clear corneal incision. Experimental measurements were performed  $81.6 \pm 24.43$  days after surgery, in a single experimental session. Spherical equivalent ranged pre-operatively from -5.75 to 1.5 D ( $-1.5 \pm 2.4$  D, on average) and post-operatively from -0.5 to 0.75 D ( $-0.125 \pm 0.5$  D, on average). The mean power of the implanted IOLs was 20.34 D (the power for each eye appears on Table 8.1). Pupils were dilated with Tropicamide 1% for the measurements. The experimental protocols followed the tenets of the Declaration of Helsinki and had been approved by Institutional Review Boards. Subjects were informed on the nature of the experiments and provided written consent.

## **2.2 Experimental measurements**

### *2.2.1 Total aberrations measurements*

Total wave aberrations were measured using a second generation laser ray tracing (LRT), which was developed at the Instituto de Óptica (CSIC) in Madrid, Spain (Llorente, Barbero, Cano, Dorronsoro & Marcos, 2004). This technique has been described and validated in detail in previous publications (Llorente, Diaz-Santana, Lara-Saucedo & Marcos, 2003, Marcos, Díaz-Santana, Llorente & C., 2002, Moreno-Barriuso, Marcos, Navarro & Burns, 2001, Moreno-Barriuso & Navarro, 2000) and was described in Chapter 1. In this technique a scanning system scans a narrow IR laser beam across the pupil. Pupil and retinal images are simultaneously captured by two CCD cameras. Ray aberrations are obtained by estimating the deviations of the centroids of the retinal spots images corresponding to each entry pupil location with respect to the reference (chief ray). These deviations are proportional to the local derivatives of the wave aberrations, which are fitted by a seventh-order Zernike polynomial expansion.

Patients' pupil diameters ranged from 4 to 6 mm, and the sampling pattern (with 37 samples in a hexagonal configuration) was adjusted by software to fit the natural pupil. In order to compare results across subjects, aberrations were scaled to the same pupil diameter (5 mm, except for subjects #4 and #12 with a pupil diameter of 4 mm). Spherical error was corrected by means of a Badal focusing system. High order aberrations are reported in terms of Zernike coefficients, using the convention of the OSA Standards (Applegate, Thibos, Bradley, Marcos, Roorda, Salmin & Atchison, 2000).

### *2.2.2 Corneal topography.*

The anterior corneal elevation was obtained using a Placido disk videokeratoscope (Humphrey-Zeiss MasterVue Atlas Model 990) which uses an arc step reconstruction algorithm (Campbell, 1997). Data were obtained over 10-mm pupils and were referred to the corneal reflex. Corneal heights were fit by a 7<sup>th</sup> order Zernike polynomial expansion and discrete points were evaluated in a XY equi-space grid, which were introduced in an optical design program (Zemax, Optima Research, 2007 Tucson) for the ray tracing evaluation (Schwiegerling, Greivenkamp & Miller, 1995). Table 1 shows three relevant coefficients (spherical, horizontal coma and trefoil) of the Zernike

polynomial expansion to the corneal height (centered at the corneal reflex and for a 10-mm pupil diameter).

### 2.2.3 Optical biometry

Anterior chamber depth (ACD) and axial length (AL) were obtained using a commercial optical biometry system (IOL master, Zeiss). This system uses anterior segment slit-lamp images to estimate ACD and low coherence interferometry to estimate AL. Table 1 shows ACD and AL in all eyes of the study.

### 2.2.4 IOL tilt and decentration.

IOL tilt and decentration were measured with a custom developed Purkinje imaging system described in detail in Chapter 2, 4 and 5 (Rosales & Marcos, 2006, Rosales, Dubbelman, Marcos & van der Heijde, 2006) and IOL tilt and decentration (de Castro, Rosales & Marcos, 2007). In brief, images of PI, PIII and PIV (first, third and fourth Purkinje Images) are obtained with eccentric (14 deg) collimated illumination from LEDs and captured on an IR CCD camera provided with a telecentric lens. The method to obtain tilt and decentration from the relative locations of PI, PIII and PIV with respect to the pupil center has also been described before. IOL tilt ( $\alpha$ ) is referred to the pupillary axis and the IOL decentration ( $d$ ) is referred to the pupil center. Sign conventions for tilt (around the horizontal and vertical axes) and decentration (horizontal and vertical) are shown in Table 8.1 and graphically depicted in Figure 2.6 and Figure 8.1.

The Purkinje imaging system was also used to estimate the relative shift of the corneal reflex (first Purkinje image) with respect to the pupil center for foveal fixation. This information was not readily available in the videokeratoscopic images obtained with our corneal topographer due to the superposition of the Placido rings with the pupil edge. For this purpose an additional channel with foveal illumination from a collimated LED was introduced in the Purkinje imaging system. In addition, we have checked that in eyes when only Purkinje images were available for eccentric illumination, similar information was achieved from extrapolations from Purkinje images positions at different fixation angles. Sign conventions for the 1st Purkinje shift (with respect to the pupil center) for foveal fixation are shown in Table 8.1. The off-axis field angle that would produce the measured shift of the first Purkinje image is obtained by virtually rotating using Phillips' linear equations. This angle is referred to the pupillary axis and

can be treated as angle  $\lambda$  (between the line of sight and pupillary axis) under the assumption that pupil decentration is small (Mandell, 1995).

All measurements with the Purkinje imaging system were performed under pupil dilation, so that it was ensured that there were no differences in the relative pupil center across the geometrical measurements obtained with this system and measurements of ocular aberrations with LRT.

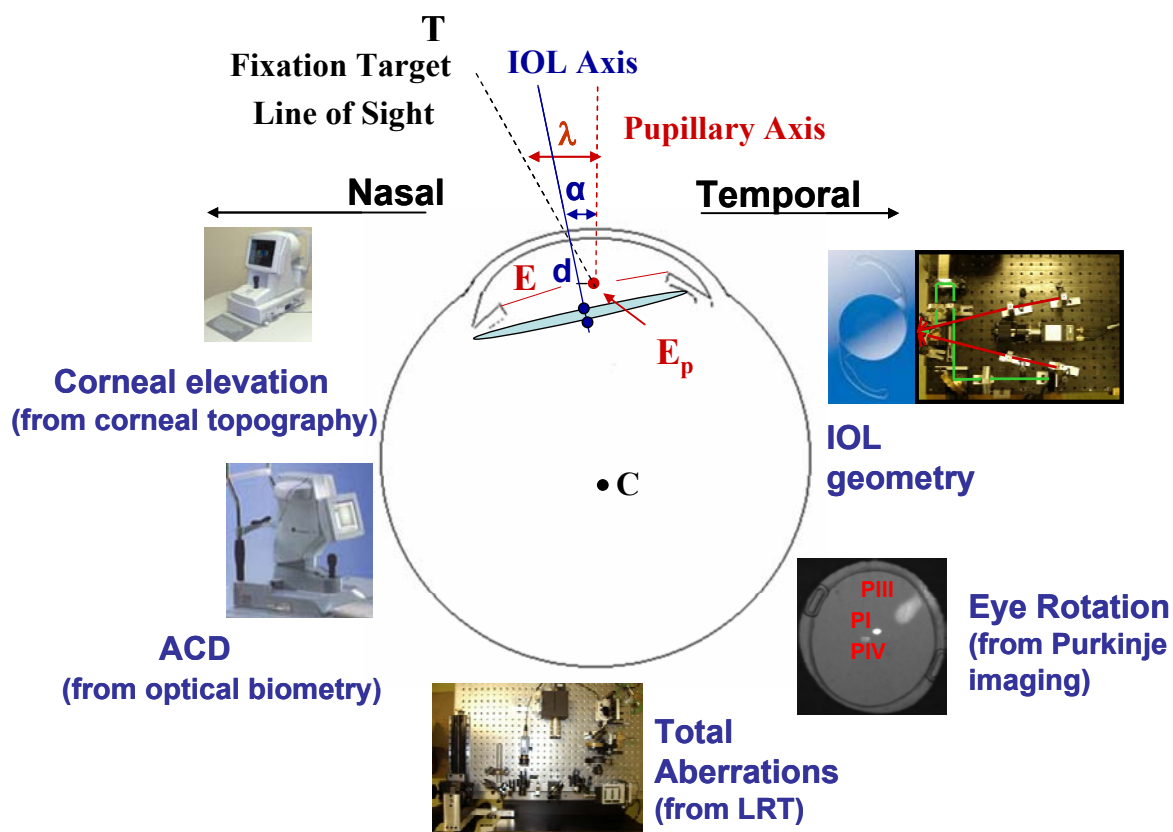


**Figure 8.1.** Schematic model eye as introduced in Zemax for numerical ray tracing and the different instruments used to obtain individual geometrical data (corneal elevation, anterior chamber depth ACD, IOL tilt and decentration) used in the model, and to measure total aberrations. The reference axes for eye rotation ( $\lambda$ ), IOL tilt ( $\alpha$ ) and decentration ( $d$ ) are shown. E stands for entrance pupil,  $E_p$  for pupil center and C for corneal center of curvature. The eye depicted represents a right eye. The line of sight is rotated nasally so  $\lambda_y$  is positive. The nasal edge of the IOL moves backward, so  $\alpha_y$  is positive. The IOL is decentered nasally, so  $d_x$  is positive.

**Table 8.1.** Individual biometrical and geometrical data used in the computer model eye.

Subject	Eye	Cornea <sup>a</sup>			ACD mm	AL mm	IOL Pow (D)	$\alpha^b$ (deg)		$d^c$ (mm)		Purkinje image shift $d^d$ (mm)		Eye Rotation <sup>e</sup> (deg)	
		$C_4^4$	$C_3^{-3}$	$C_4^0$				x	y	x	y	x	y	x	y
		$\mu\text{m}$	$\mu\text{m}$	$\mu\text{m}$											
S1	#1 (OD)	-2.4	4.4	-9.2	4.00	23.3	19.5	-1.74	0.98	0.31	0.06	0.53	-0.24	1.82	4.06
	#2 (OS)	-2.1	2.06	-2.2	4.57	23.7	19.5	-1.78	-0.22	-0.28	-0.01	-0.77	-0.19	1.51	-5.92
S2	#3 (OD)	-2.9	1.46	-11	4.11	23.1	20	-1.19	0.98	0.52	-0.12	0.35	-0.11	0.83	2.74
	#4 (OS)	-2.1	0.8	-7.8	3.87	22.8	19.5	-0.90	-0.75	0.19	-0.28	-0.72	0.14	-1.12	-5.71
S3	#5 (OD)	0.12	-4.2	0.6	4.52	23.5	19.5	-0.53	1.78	0.30	-0.02	0.39	0.12	-0.94	2.97
	#6 (OS)	-0.2	-5.5	1.03	2.29	23.1	21.5	2.12	-1.72	-0.23	-0.03	-0.55	0.27	-2.04	-4.19
S4	#7 (OD)	-0.9	-0.8	16.6	4.56	23.9	21	-2.94	1.08	0.27	-0.40	0.32	-0.20	1.55	2.49
S5	#8 (OD)	-1.3	0.5	-14	4.45	22.9	18.5	0.90	1.18	0.51	-0.15	0.27	0.08	-0.61	2.16
	#9 (OS)	-3.0	-1.1	-35	4.40	22.6	21.5	-1.07	-0.07	-0.27	0.26	-0.38	0.06	-0.51	-3.12
S6	#10 (OD)	-2	-2.1	2.9	3.31	24.4	20	-3.39	2.31	0.20	0.53	0.54	0.17	-1.21	3.94
	#11 (OS)	-1.7	-5.8	2.59	4.88	24.4	19	-1.84	-2.60	-0.31	-0.30	-0.36	0.17	-1.27	-2.62
S7	#12 (OD)	-0.6	-2.6	0.64	3.57	21.2	24.5	0.07	1.28	0.38	0.21	0.43	0.27	-2.27	3.48

a.- Corneal heights are fit to a 7<sup>th</sup> order Zernike polynomial. The table shows three relevant terms as examples.

b.- Tilt x ( $\alpha_x$ ) stands for tilt around x (or vertical tilt). Sign conventions are: Positive, superior edge of the lens is closer to the cornea than the inferior edge, and vice versa for Negative. Tilt y ( $\alpha_y$ ) stands for tilt around y (or horizontal tilt). Sign conventions are: Positive, nasal edge of the lens moves backward (for the right eye) or forward (for the left eye), and viceversa for Negative.

c.- Decentration x ( $d_x$ ) stands for horizontal decentration. Sign conventions are: Positive, the lens is shifted toward the nasal (right eye) or temporal (left eye) direction and viceversa for Negative. Decentration y ( $d_y$ ) stands for vertical decentration. Sign conventions are: Positive, the lens is shifted upward and viceversa for Negative.

d.-Purkinje image shift x stands for a horizontal shift. Sign conventions are: Positive, the Purkinje image is shifted toward the nasal direction and viceversa for negative. Purkinje image shift in y stands for vertical decentration. Sign conventions are: Positive, the Purkinje image is shifted upward and viceversa for negative.

e.-Eye rotation. Rotation x stands for rotation around x (or vertical rotation). Sign conventions are: Positive, the line of sight is rotated upwards with respect to the pupillary axis, Negative, the line of sight is rotated downwards referred to the pupillary axis. Rotation y stands for rotation around y (or horizontal rotation). Sign conventions are: Positive, the eye rotates to the nasal (right eye) or temporal side (left eye) and viceversa for the Negative. The eye center rotation is considered at 15 mm behind the cornea.

### *2.2.5 Computer simulations*

Customized eye models were built using the Zemax (Focus Software, Tucson, AZ, Zemax, January 2006 ) optical design program, where an optical system is defined as a sequential group of surfaces separated by refractive index media.

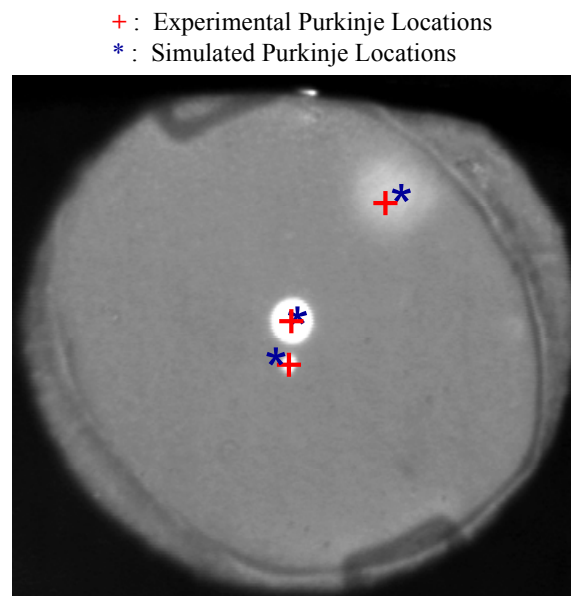
The anterior corneal surface was obtained from videokeratoscopy and modeled with the grid sag surface type within the Zemax program. For the posterior corneal surface, a standard spherical surface with a radius of 6.5 mm was used. Corneal refractive index was taken as 1.376. The IOL anterior and posterior surface geometry was provided by the manufacturer, and introduced in the model eye as standard conic surfaces, with the nominal thickness and refractive index of the lens. Measured values of tilt and decentration of the IOL are introduced with respect to the pupillary axis. Finally, the whole eye is rotated to simulate off-axis measurements obtained due the eccentric location of the fovea.

Figure 8.1 shows the schematic diagram of the model eye introduced in Zemax for the simulations and the different instruments used to measure corneal shape, ocular biometry, lens tilt and decentration and ocular aberrations. We have verified that the relative positions of the ocular surfaces and eye rotation for foveal fixation are correct by simulating in Zemax the locations of PI, PIII and PIV for the model eye and compared them to the real measurements for foveal fixation. Figure 8.2 shows a good agreement between simulated and experimental locations of the Purkinje images for the model eye at foveal fixation.

The simulations of ocular aberrations were performed for a wavelength of 786 nm. The index dependence of the wavelength is introduced fitting experimental longitudinal chromatic aberration with Herzberger formula (Herzberger, 1969). Aberrations were evaluated at best focus (defined as the location where the spot diagram is most compact), since aberrations were measured for best spherical correction. A sampling matrix of 64x64 rays was used to calculate the aberrations.

In order to assess the relative contribution of different factors to ocular wave aberrations, the simulations are performed for the cornea alone, for the cornea and the IOL (assuming no tilt and decentration, i.e. aligned with respect to the pupillary axis), and for the cornea and the IOL with the measured tilt and decentration. All simulations were referred to the pupil center, and accounting for the misalignment of the videokeratoscopic axis and the line of sight (i.e, with a field angle for incoming rays

accounted for by angle  $\lambda$ ). Comparisons between simulated (using customized eye models) and measured (with LRT) aberrations were performed in terms of correlations between the sets of simulated and measured Zernike terms (slope and regression coefficient of linear correlations) for each eye, and comparisons of individual Zernike terms for all eyes.



**Figure 8.2.** Simulated and experimental Purkinje images locations for the eye model depicted in A (for foveal fixation).

### 2.2.6 Physical eye model and computer simulations

Additional assessment of the accuracy of the virtual eye model to predict wave aberrations was performed using a physical model eye with aspheric and spherical IOLs of several powers (18, 21, 23,5 and 26 D). This model eye had been used in a previous study (chapter 5) for validations of the measurements of IOL tilt and decentration with Purkinje and Scheimpflug imaging system (de Castro et al., 2007). It consists of a PMMA water cell model, with a spherical PMMA contact lens simulating the cornea and IOL lenses on a XYZ micrometer stage and rotational stage. Nominal values of anterior (7.80 mm), posterior corneal radius (6.48 mm) and central thickness (500  $\mu\text{m}$ ) were checked with standard contact lens calibration equipment and corneal topography. Decentration was achieved in the horizontal direction, with a precision of 0.1 mm and ranged from 0 to 1 mm. Tilt of the IOL was achieved in the horizontal direction with a precision of 0.01 degrees, and ranged from 1 to 4 deg. Eye rotation was achieved in the

horizontal direction with a precision of 0.1 degree, and was set constant to 5 deg. Anterior chamber depth was variable with a precision of 0.1 mm, and ranged from 3.5 to 5.5 mm. A total of 31 combinations of the former were tested, by measuring total aberrations with the LRT and simulating aberrations by numerical ray tracing in Zemax for each condition.

### **3. RESULTS**

#### **3.1 Individual geometrical data.**

Table 8.1 shows the geometrical data measured for each eye and used in Zemax to simulate the optical aberrations. Relevant terms of corneal topography, anterior chamber depth from optical biometry, IOL power from clinical records, IOL tilt and decentration, 1<sup>st</sup> Purkinje image shift and eye rotation from Purkinje imaging are listed. Measurement error has not been introduced in the Table 1. The average standard deviations of repeated measurements were  $0.27\pm 0.21$ deg (around x-axis) and  $0.35\pm 0.22$  deg (around y-axis) for IOL tilt,  $0.09\pm 0.07$ mm (x) and  $0.05\pm 0.03$ mm (y) for IOL decentration, and  $0.14\pm 0.11$ deg (around x-axis),  $0.07\pm 0.06$  deg (around y-axis) for eye rotation and 0.08 mm for ACD.

#### **3.2 Wave aberrations. Simulations vs real measurements.**

Figure 8.3 shows examples of measured (first column) and simulated (column 2-4) wave aberrations in four subjects (eyes #2, #3, #6, #11) for 3<sup>rd</sup> and higher order aberrations (i.e, excluding tilt, defocus and astigmatism), and for a pupil diameter of 5 mm. The second column (Cornea) represents a simulation of the wave aberration of the eye without the IOL, (i.e shows the aberrations of the cornea alone), the third column (Cornea +IOL) shows the total wave aberration of the eye with the IOL assuming that the IOL is perfectly aligned with respect to the pupillary axis, and the forth column (Cornea + IOL Tilt and decentration) represents the total wave aberration of the eye with the IOL tilted and decentered according to the measured tilts and decentrations. In the three cases, the eye is rotated according to angle  $\lambda$  in order to incorporate the line-of-sight misalignment. In general, the corneal wave aberration map shows many of the relevant features of the measured wave aberrations. The similarity is slightly improved when the IOL is included, and marginally further improved in some cases when IOL tilts and decentrations are added.

Comparisons of measured and simulated aberrations were performed using linear correlations between total and simulated Zernike terms, eye by eye. The accuracy of the model as well as the relative importance of each factor (corneal topography, IOL geometry and IOL tilt and decentration) is assessed from the slopes and correlation coefficients of these linear regressions (closest to 1 indicated better prediction). Figure 8.4 shows the linear correlations between measured and simulated Zernike terms (excluding tilt and defocus) for the eyes in Figure 8.3 and the corresponding linear regressions. All data are for 5 mm pupil diameters.

The slope values are shown in Table 2. Ideally, a perfect correlation would have a slope of one. Table 3 shows regression coefficients for the fitted linear regressions in each eye, including astigmatism for the Cornea alone model (A), Cornea + IOL (B) and Cornea + IOL with tilt and decentration (C). Except for one eye (#4) there are significant correlations ( $p < 0.0001$ ) with high regression coefficients in all cases, even in the cornea-alone model. The slope decreases when the IOL is incorporated (from case A to case B), found in 9 of 12 eyes is indicative of the corrective effect of IOL (with an aspheric design to counteract the positive spherical aberration of the cornea). Predictions are improved (the slope gets closer to one) when real tilt and decentration of the IOL are included in the model in 6 of the eyes. We did not find a significant correlation between the amount of improvement with tilt and decentration and the magnitudes of tilt and decentration.

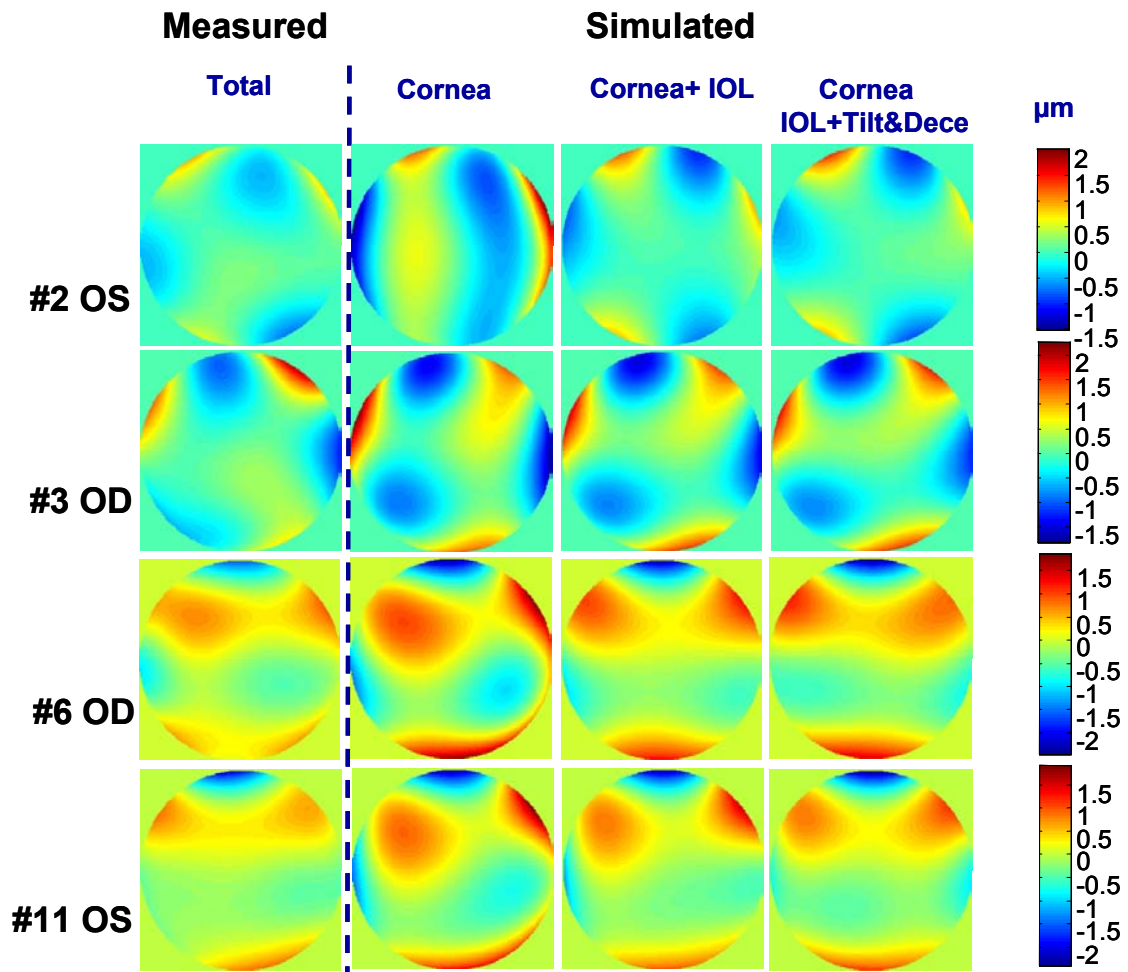


**Figure 8.3.** Examples of measured and simulated wave aberrations in four eyes for 3<sup>rd</sup> and higher order aberrations First Column: Measured aberration with Laser ray tracing. Second column: Simulated aberrations with the cornea only (rotated by angle  $\lambda$ ), Third column: Simulated aberrations for the model eye with cornea and the corresponding IOL design, Fourth column: Simulated aberrations for the model eye with cornea and IOL introducing the measured tilt and decentration.

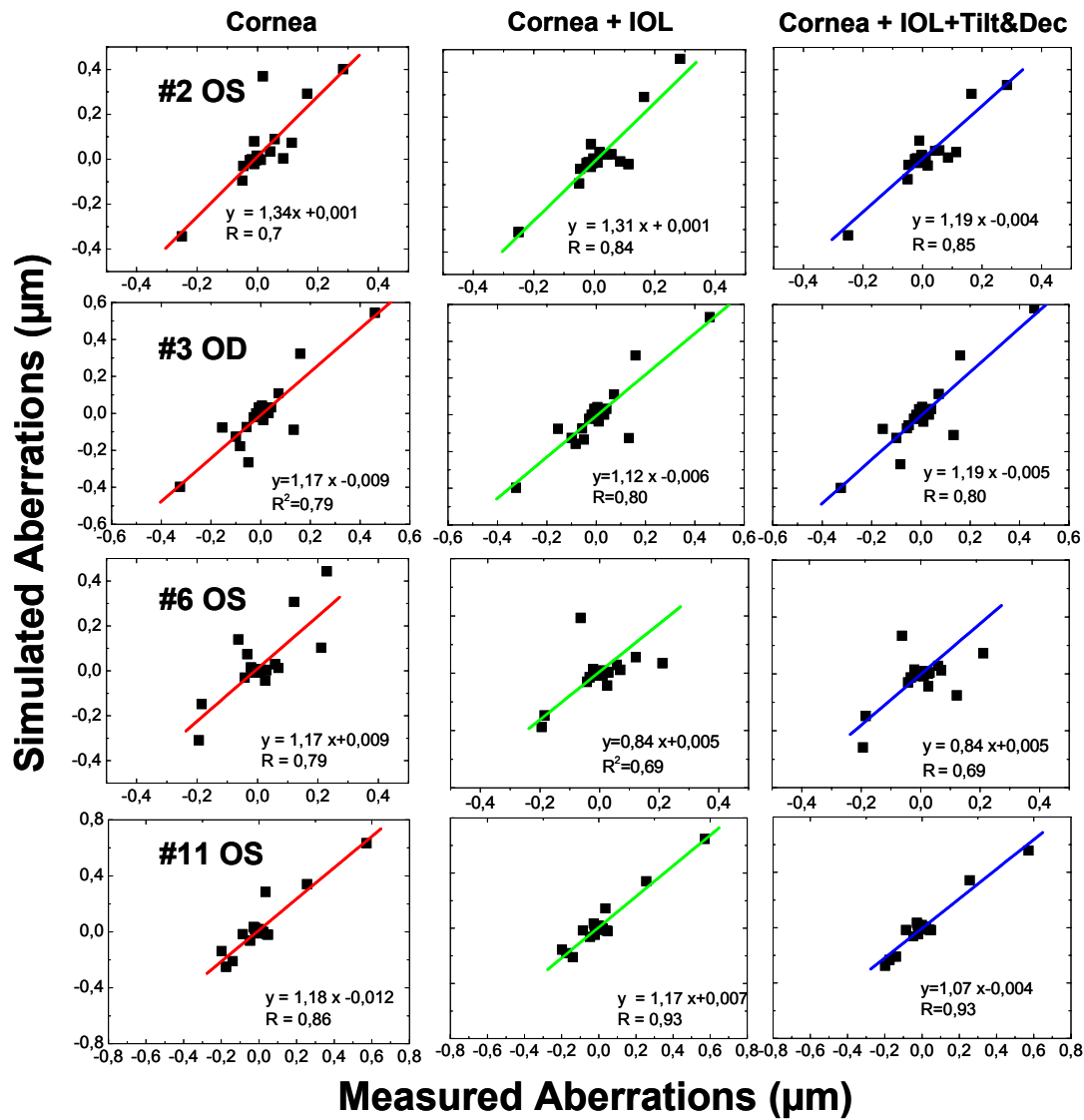


**Figure 8.4.** Linear correlations between measured and simulated aberrations (only cornea, first column; cornea and IOL, second column; cornea and IOL introducing tilt and decentration, third column), for the examples of Fig. 3. All Zernike terms (except for defocus and tilt) are included. Data are for 5 mm pupil diameters.

**Table 8.2.** Slopes of the linear correlation between measured and simulated Zernike coefficients, for each eye (including astigmatism)

	SUBJECT/EYES												
	S1		S2		S3		S4		S5		S6		S7
	#1	#2	#3	#4	#5	#6	#7	#8	#9	#10	#11	#12	
	(OD)	(OS)	(OD)	(OS)	(OD)	(OS)	(OD)	(OD)	(OS)	(OD)	(OS)	(OD)	
<b>A<sup>a</sup></b>	1.28	1.34	1.17	0.67	0.88	1.17	1.34	1.74	2.10	1.48	1.12	2.51	
<b>B<sup>b</sup></b>	0.93	1.31	1.12	0.15	0.85	0.84	1.34	1.72	2.07	1.51	1.11	2.54	
<b>C<sup>c</sup></b>	0.94	1.20	1.19	-0.02	0.81	0.89	1.34	1.88	2.13	1.53	1.07	2.19	

- a.- Simulated aberrations with only cornea
- b.- Simulated aberrations with cornea and IOL
- c.- Simulated aberrations with cornea and IOL with tilt and decentration

**Table 8.3.** Regression coefficients of the linear correlation between measured and simulated Zernike coefficients for each eye (including astigmatism)

	SUBJECT/EYES												
	S1		S2		S3		S4		S5		S6		S7
	#1	#2	#3	#4	#5	#6	#7	#8	#9	#10	#11	#12	
	(OD)	(OS)	(OD)	(OS)	(OD)	(OS)	(OD)	(OD)	(OS)	(OD)	(OS)	(OD)	
<b>A<sup>a</sup></b>	0.73	0.84	0.89	0.49	0.73	0.79	0.98	0.92	0.93	0.87	0.93	0.78	
<b>B<sup>b</sup></b>	0.76	0.92	0.90	0.14	0.80	0.69	0.99	0.93	0.93	0.90	0.97	0.80	
<b>C<sup>c</sup></b>	0.69	0.92	0.90	-0.02	0.73	0.71	0.98	0.90	0.93	0.92	0.96	0.79	

- a.- Simulated aberrations with only cornea
- b.- Simulated aberrations with cornea and IOL
- c.- Simulated aberrations with cornea and IOL with tilt and decentration

The average values for the slopes across the 12 eyes, including astigmatism, were  $1.4 \pm 0.51$  (Cornea),  $1.29 \pm 0.63$  (Cornea + IOL),  $1.26 \pm 0.62$  (Cornea + IOL Tilt and decentration). While the correspondence between simulated and measured aberration coefficients is good in most eyes, there is an overestimation of the simulated coefficients as compared to the measured ones, particularly in eyes #8, #9, #10 and #12. We have repeated the correlation analysis excluding astigmatism and found average values for the slopes of  $0.82 \pm 0.33$  (Cornea),  $1.07 \pm 0.5$  (Cornea + IOL),  $1.1 \pm 0.45$

(Cornea + IOL Tilt and decentration). In general, we found smaller slopes and closer to 1 when astigmatism is not included.

### 3.3 Individual Zernike coefficients.

We compared measured and simulated individual Zernike coefficients. Correlations between simulated and measured astigmatism are high ( $r= 0.97\pm 0,33$  for astigmatism at 0/90 deg,  $Z_2^2$ , and  $0.88 \pm 0,2$  for oblique astigmatism,  $Z_2^{-2}$ ). There is a consistent overestimation of the simulated astigmatism by 17.3% for  $Z_2^2$  and by 8.7% for  $Z_2^{-2}$ , with respect to the real measurements. The results for the cornea alone are similar to those with the model with the IOL (either lined up or tilted/decentered), indicating that the cornea is the only source of astigmatism in pseudophakic eyes, and IOL tilt and decentration play a negligible role in the post-operative astigmatism. Figure 5 shows 4<sup>th</sup> order spherical aberration for the simulated and real eyes. Data are for 5 mm pupil diameter, except for subjects #4 and #12 with a pupil diameter of 4 mm. The presence of the aspheric IOL reduces the spherical aberration of the eye, with respect of that of the cornea in all eyes, as previously reported (Barbero et al., 2003). As revealed by both the simulations and real measurements, eyes with the highest amounts of corneal spherical aberration present the highest amount of total spherical aberration (eyes #8 and #9).

However, eyes with similar amounts of corneal spherical aberration (for example #4 and #6) may result in very different total spherical aberration (positive in eye #4 and negative in #6) depending on other anatomical factors, as revealed by both the simulations and real measurements. In general, the eye model predicts the individual variability across eyes and captures the individual trends for spherical aberration found in each eye.

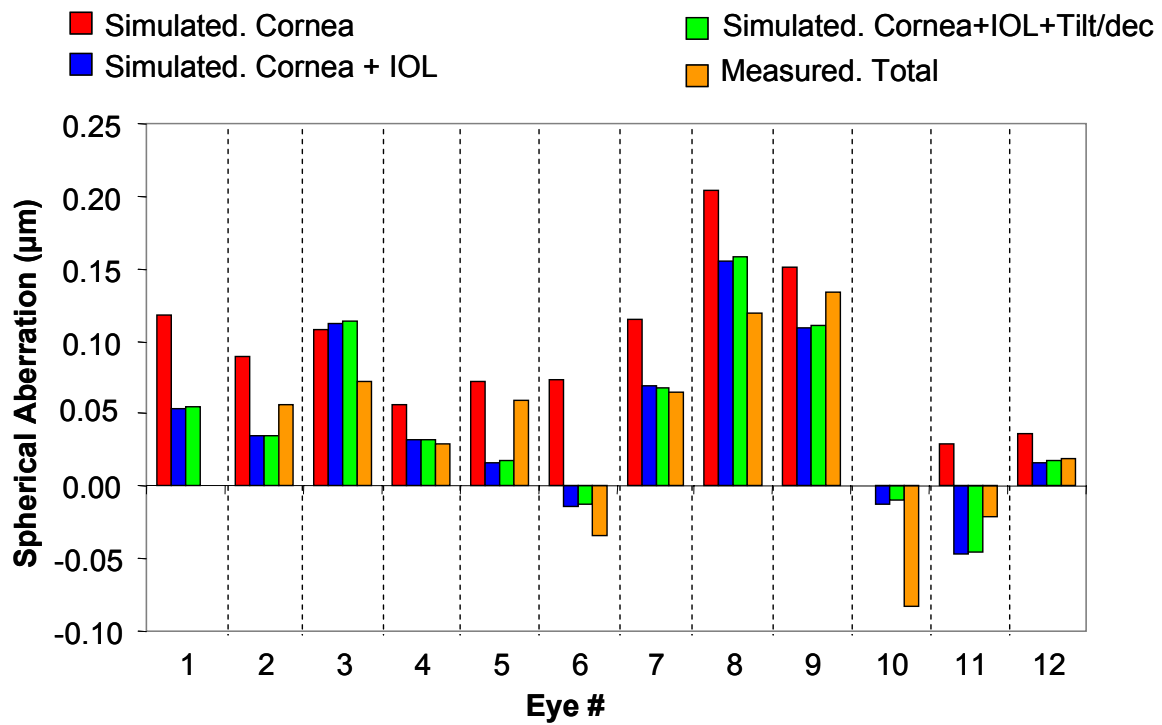


Figure 8.5. 4<sup>th</sup> order spherical aberration for the simulated and real eyes.

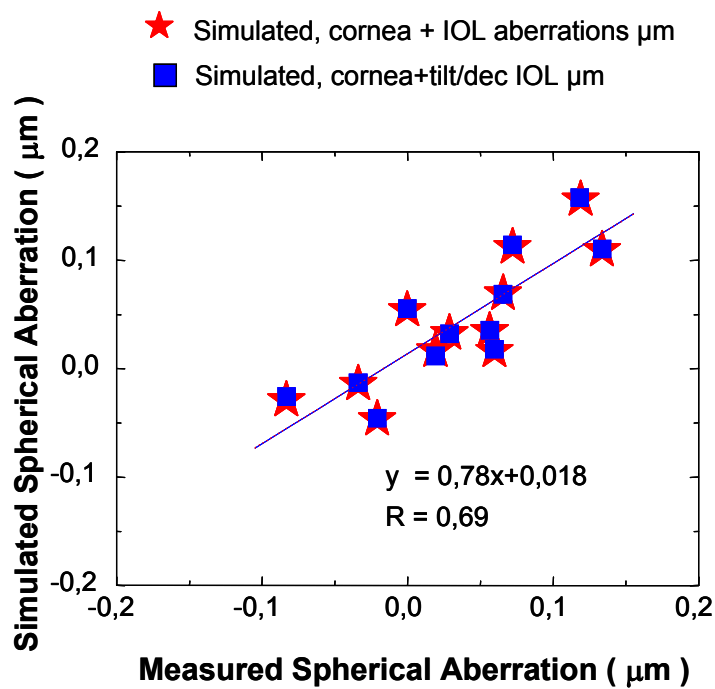


Figure 8.6. Simulated vs measured spherical aberration, for all eyes.

Figure 8.6 demonstrates a high correlation between the simulated spherical aberration of the complete eye model versus the experimental data in Figure 5. The spherical aberration is also close to zero, as expected from the intended design of the aspheric IOL. The simulations also indicate that presence of IOL tilt and decentration does not affect total spherical aberration.

Figure 8.7 shows horizontal coma for the simulated and real eyes. Horizontal coma is reduced in all eyes with respect to corneal values, as shown by both simulated and real data (with a decrease between 5% and 35%). Right/Left eye mirror symmetry is found for the cornea in all pairs of eyes, with negative coma in right eyes and positive in left eyes. This symmetry is found only in three out of the five pairs of eyes for total coma. While the effect of the IOL to reduce the corneal horizontal coma is already captured with the model with centered IOLs, incorporating the actual amounts of IOL tilt and decentration improves the accuracy of the model in 7 out the 12 eyes, and the trends are captured in all eyes except #6 and #9, where the shift of coma when tilt and decentration are incorporated goes in different directions in simulated and real data. Interestingly, in most eyes (1, 2, 3, 5, 10, 11 & 12) the presence of tilt and decentration not only is not associated with larger amounts of horizontal coma, but this is further reduced (10%) with respect to a centered lens.

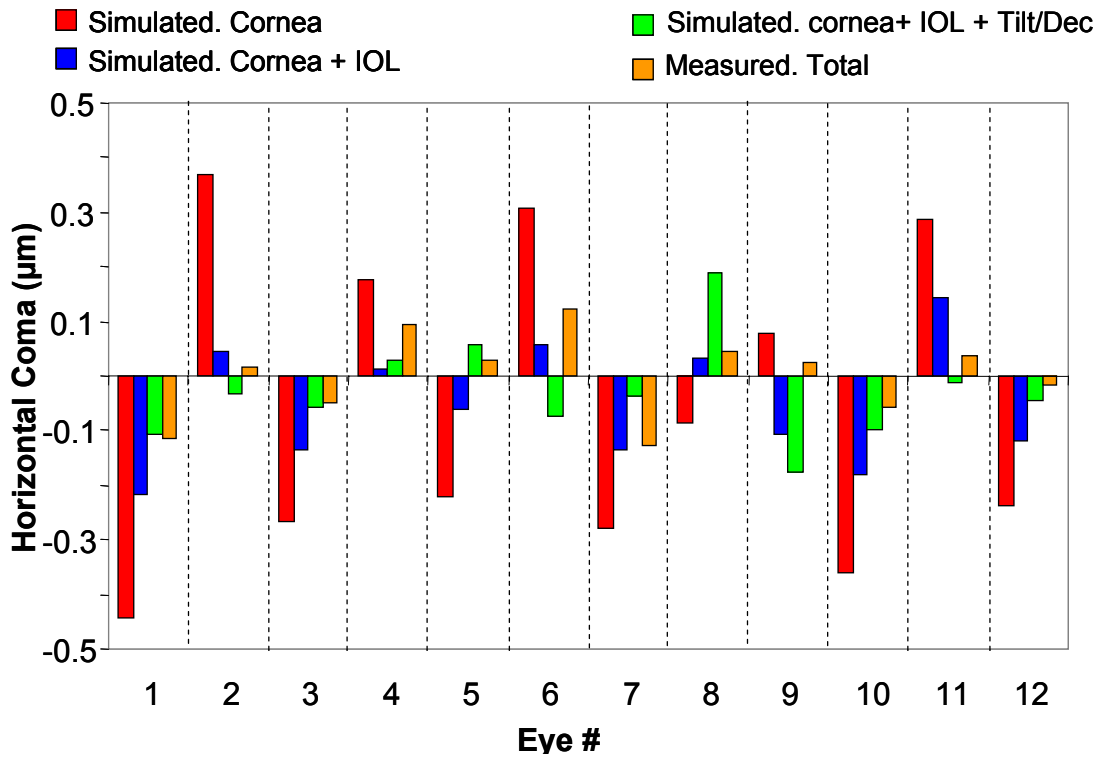


Figure 8.7. Horizontal coma obtained for the simulated and real eyes.

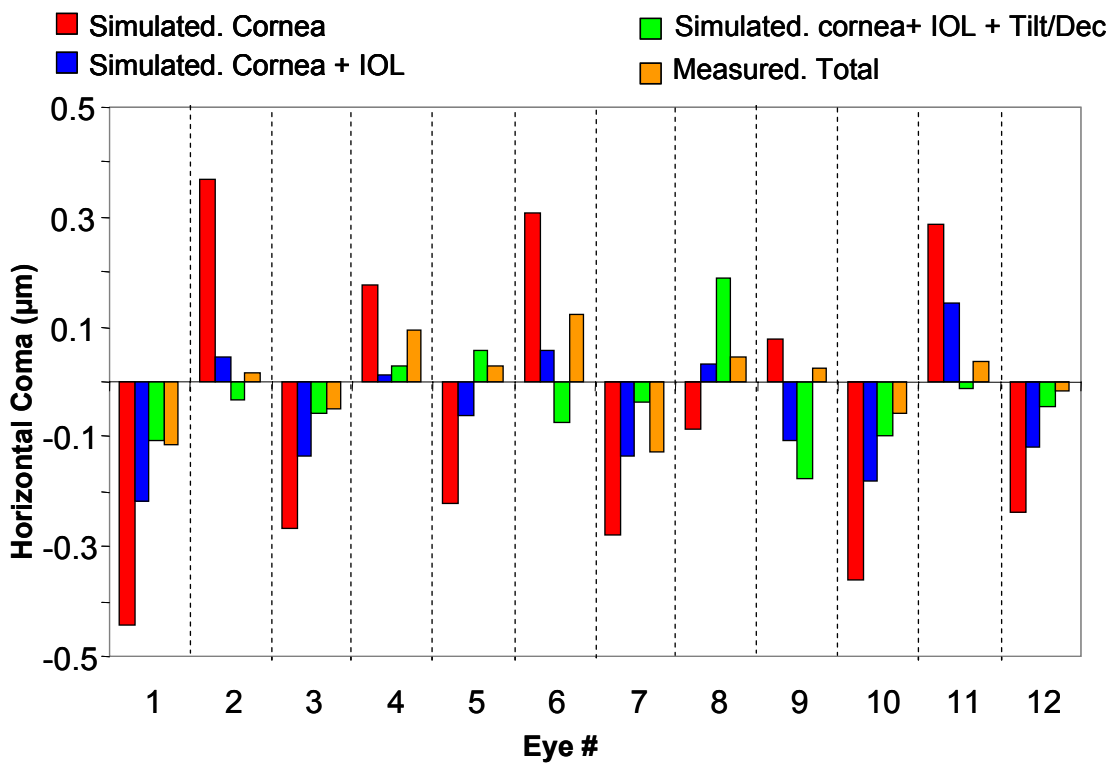


Figure 8.8. Vertical Trefoil obtained for simulated and real eyes.

Figure 8.8 shows vertical trefoil for all eyes. This is a relevant aberration, which has been shown to be induced in the cornea by cataract surgery. The correlation between experimental vs simulated data is significant both for vertical (slope=1  $r=0.58\pm 0.15$   $p=0.05$ ), and horizontal trefoil (slope=1.25  $r=0.74\pm 0.15$  and  $p=0.003$ ). The discrepancies are larger for vertical than for horizontal trefoil, although we could not find a systematic over or underestimation from the model with respect to real measurements.

#### 4. DISCUSSION

We have presented a customized computer eye model, using individual geometrical data in eyes with intraocular lenses, which reproduces the wave aberrations measured in the same eyes. We have evaluated the contribution of the different factors (corneal topography, IOL geometry, IOL misalignments, eye rotation) to the wave aberration and demonstrated the interactions between those that result in the measured ocular aberrations. The study of the accuracy and limitations of the model is important to address further applications. The detailed evaluation of the relative contributions of anatomical factors to global optical quality in eyes with IOLs is important for the improvement of IOL design and surgical strategies.

##### 4.1 Validation of the eye model and limitations.

We have found a good correspondence between simulated and measured aberrations. The accuracy of the prediction is in general improved when IOL geometry and actual measurements of IOL tilt and decentration are incorporated. While the correlations are high in all eyes but one (coefficients of correlation of 0.78 on average), the overall predicted aberrations seem to overestimate slightly the measured values, with an average slope (predicted vs measured) of 1.22 across all eyes (see Table 2), particularly when astigmatism is included. This overestimation seems also to occur in a recent study by Tabernero et al. (Tabernero, Piers, Benito, Redondo & Artal, 2006) on eyes with spherical ( $n=3$ ) and aspheric IOLs ( $n=4$ ), where a correlation pooling Zernike coefficients (including astigmatism) of all eyes (rather than studying eye by eye) yielded a slope of 0.89 (measured vs predicted). For the spherical aberration term, neither Barbero (Barbero et al., 2003), Tabernero (Tabernero, et al, 2006) or our study show a systematic deviation.

Our model uses a generic posterior corneal spherical surface. Other customized models (Barbero et al., 2003) used one-surface cornea. However, contributions of the posterior corneal shape to corneal astigmatism in particular have been shown. In general it has been found that astigmatism arising from the corneal surface is reduced by astigmatism of the opposite sign arising from the posterior corneal surface (Dubbelman, Sicam & van der Heijde, 2006, Dunne, Royston & Barnes, 1991, Prisant, Hoang-Xuan, Proano, Hernandez, Awad & Azar, 2002). A study by Dunne et al (Dunne, Royston & Barnes, 1991) in a group of 60 young subjects (mean age  $22.04 \pm 3.24$  years old) showed that the toricity of the posterior corneal surface, if it was purely governed by that of the anterior surface, would produce a reduction of total corneal astigmatism of about 5%, however, if the additional toricity of the posterior cornea was taken into account, total corneal astigmatism would be reduced by approximately 14%. Dubbelman (Dubbelman et al., 2006) using Scheimpflug imaging on 114 subjects, ranging in age from 18 to 65 years, showed that the astigmatism of the posterior corneal surface compensates the astigmatism of the anterior corneal surface by 31%. These results are consistent with our findings comparing total and simulated astigmatism .

Other than the simplified posterior corneal surface, the origin of systematic changes could arise from some assumptions in our model regarding the corneal refractive index (rather than a more complex gradient index of refraction (Barbero, 2006)) or the use of simplified spherical posterior corneal surface (rather than using the actual posterior corneal topography) or deviations associated with the techniques themselves. We verified that simulated aberrations did not deviate systematically from real aberrations in the artificial physical model eye described in Section 2.2.6, for which all geometrical and optical properties (including posterior “corneal” shape and index of refraction) are known. Correlations between simulated and measured Zernike terms yielded a slope of 1.03 on average (averaging across 31 different configurations of the physical model eye). This result suggests that there are not systematic errors associated to the aberration measurement technique neither in the computer eye modeling algorithms. Other sources of discrepancies between simulated and real aberrations can come from errors in the ACD measurement with the IOLmaster, which have been reported to be higher in aphakic eyes (Kriechbaum, Findl, Kiss, Sacu, Petternel & Drexler, 2003), or slight pupil shifts (between the LRT measurement and the Purkinje pupillary image), along with experimental errors of IOL tilt and decentration, corneal topography and aberrometry. We have estimated the standard deviation of the simulated aberrations, based on typical

measurement variability of corneal topography, ACD and geometrical measurements (angle  $\lambda$ , tilt and decentration). We found a standard deviation of 0.0047  $\mu\text{m}$  for the simulated spherical aberration and 0.005  $\mu\text{m}$  for 3<sup>rd</sup> and higher order RMS. These values are smaller than the standard deviations of real aberration measurements (0.02  $\mu\text{m}$  and 0.03  $\mu\text{m}$  respectively).

The customized computer eye model relies on the correct location of the optical surfaces of the ocular components with respect to the reference axes of the eye. We have used the location of the 1<sup>st</sup> Purkinje image for foveal fixation to obtain the angle  $\lambda$ . Tilt and decentration were obtained from Purkinje images obtained with eccentric illumination. Comparisons of the locations of PI, PIII and PIV from real images and simulations using the customized eye models for foveal fixation verified that the relative alignment of ocular surfaces was correct (see Figure 8.2). An assumption in our model is that the shift of the 1<sup>st</sup> Purkinje image from the pupil center for foveal fixation is solely due to the tilt of the line of sight with respect to the videokeratoscopic axis, while a pupil decentration may also occur. The contributions of each to the shift of 1<sup>st</sup> Purkinje image cannot be separated in our measurements and therefore cannot be separately introduced in the model. Our previous computer eye model with IOLs (Barbero et al., 2003) did not incorporate angle  $\lambda$ , and the recent study by Tabernero (Tabernero et al., 2006) seems to have attributed all the shift of videokeratoscopic axis to lateral decentration. We repeated the simulations for all 12 eyes assuming just decentration and obtain little differences in terms of the metrics used to assess the accuracy of the model (an average slope of 1.18 and a regression coefficient of 0.77).

#### **4.2 Relative contribution of cornea, IOL geometry and misalignment to eye rotation to ocular aberrations.**

The measurement of ocular aberrations in pseudophakic eyes allow assessment of the overall optical performance (Barbero et al., 2003). The use of customized model eyes with individual geometrical data of the eyes, in combination with the actual measurements of ocular aberrations can be used to identify the relative importance of each factor. Our results show that 70% of the variance of ocular aberrations in eyes with aspheric IOLs can be predicted just from the cornea. Given the changes induced by small-incision cataract surgery on corneal aberrations (see Chapter 7) the actual post-operative corneal elevation should be used in the model. The use of individual posterior

corneal topography would likely further improve the accuracy of the model particularly for astigmatism and perhaps trefoil. The aspheric geometry of the IOL plays an important role in balancing corneal spherical aberrations. The customized eye model also helps to understand the different amounts of spherical aberration compensation found in different eyes, even for similar amounts of corneal spherical aberration. The eye rotation introduced in the model to compensate the videokeratoscope-line-of sight misalignment appears to be the cause of compensation of off-axis horizontal coma, as previously reported in normal young eyes (Tabernero, Piers, Benito, Redondo & Artal, 2006). Both the simulated and real measurements of our study suggest that this effect also happens in pseudophakic eyes with aspheric IOLs. In addition, the customized eye model has revealed that IOL tilt and decentration play a very limited role in the overall aberrations (predicting less than 2.2% of the variance), at least in this group of eyes. Higher amounts of tilts and decentrations, accounted for separately, are uncorrelated to higher amounts of relevant aberrations such as coma, confirming previous suggestions that the actual combinations of tilt, decentration, and also eye rotation are essential, and simulations using simple eye models are insufficient (Barbero et al., 2003). In fact, we have found that in 7 of the 12 eyes of this study the presence of tilt and decentration of the IOL actually results in further compensation of the off-axis coma.